

Hierarchical Co_3O_4 Nanowires as Binder Free Electrodes for Reversible Lithium Storage

Zichao Zhang,^a Li Li,^{*,a,b} Quan Ren,^a Qi Xu,^a and Bingqiang Cao^{*,a}

^a Key Laboratory of Inorganic Functional Materials in Universities of Shandong, School of Materials Science and Engineering, University of Jinan, Jinan, Shandong 250022, China

^b Key Laboratory of Advanced Energy Materials Chemistry (Ministry of Education), Nankai University, Tianjin 300071, China

To develop a long cycle life and good rate capability electrode, tricobalt tetraoxide (Co_3O_4) nanowires with hierarchical structure composed of ultra-small nanoparticles are directly grown on nickel foam current collector. The size of the nanoparticles is about 10 nm. They are synthesized via a facile hydrothermal route followed by calcination and evaluated as an anode of binder-free lithium-ion batteries. The concentration of reactant and duration of reaction are considered as important synthesis parameters. Co_3O_4 nanowires electrode exhibits excellent electrochemical performance including outstanding cycling performance, a high reversible discharge capacity and good rate capability, owing to the hierarchical architecture composed of micro-/nanostructures. After rate capacity performance measurements, a capacity of $1060.1 \text{ mAh}\cdot\text{g}^{-1}$ is retained. At a rate of $500 \text{ mA}\cdot\text{g}^{-1}$, a reversible capacity remains stable as high as $957 \text{ mAh}\cdot\text{g}^{-1}$. The enhanced performance is owing to the hierarchical structure of the nanowires and good contact with the substrate which can make electrons efficiently transport from Co_3O_4 nanowires to the current collectors. The mesoporous structure may facilitate the lithium ion diffusion and mitigate the internal mechanical stress induced by volume variations of the electrode upon cycling, which lead to outstanding electrochemical performance.

Keywords hierarchical, Co_3O_4 nanowires, binder-free, electrochemical performance

Introduction

To cope with the intermittence of renewable sources of power, such as wind, solar energy, etc. and meet the demand of mobile power for portable devices, rechargeable lithium-ion batteries (LIBs) are considered as the dominant energy storage systems.^[1-6] However, low theoretical capacity and lower power density of commercially used graphite anode limit its further application in high energy and high power devices. Significant efforts have been made to overcome this limitation and to achieve super performances LIBs with long cycle life. The electrode material is generally believed to dominate electrochemical properties and battery performances.^[7-11] In this situation, transition metal oxides (TMOs) have attracted more and more attention, due to their higher theoretical capacity.^[12,13] Among various TMOs, Co_3O_4 is becoming research hotspots owing to its high theoretical capacity of about $890 \text{ mAh}\cdot\text{g}^{-1}$. Different with the intercalation reaction mechanism of graphite, TMO_x can interact with Li based on the conversion mechanism ($\text{MO}_x + 2x\text{Li} \leftrightarrow \text{M} + x\text{Li}_2\text{O}$).^[14,15] Co_3O_4 can store more lithium atoms and deliver multi-

ple electrons during the redox reaction process.^[16-20] Investigations of Co_3O_4 have been focused on increasing the specific capacity, long-time cycle performance and reversible capacity through designing and implementing Co_3O_4 nanostructures.

The obstacles like poor conductivity and structural disintegration during the charge-discharge processes result in poor rate capability. To address these challenges, many strategies have been reported. First, one general accepted strategy to improve electrochemical performance is to use the carbon material such as graphite, graphene, carbon nanofiber/nanosheet to scatter Co_3O_4 . Liu *et al.*^[21] prepared uniform $\text{Co}_3\text{O}_4/\text{C}$ hollow quasi-nanospheres and achieved a capacity of $629 \text{ mAh}\cdot\text{g}^{-1}$ at $1780 \text{ mA}\cdot\text{g}^{-1}$. Sun *et al.*^[22] successfully synthesized a novel anode material consisting of mesoporous Co_3O_4 nanosheets-3D graphene networks which exhibited high reversible capacity. Peng *et al.*^[23] designed and synthesized hollow nanoparticles encapsulated in a thin carbon nanosheet array that exhibited stabilized specific capacity ($\sim 1052 \text{ mAh}\cdot\text{g}^{-1}$ at $0.1 \text{ A}\cdot\text{g}^{-1}$). And many other excellent researches also achieved the high capacities. Another effective strategy is to fabricate

* E-mail: mse_lil@ujn.edu.cn; Tel.: 0086-0531-89736292

Received December 3, 2015; accepted January 18, 2016; published online March 23, 2016.

Supporting information for this article is available on the WWW under <http://dx.doi.org/10.1002/cjoc.201500848> or from the author.

nano/microstructured materials with one-dimensional, two-dimensional and three-dimensional structures. Among these reported nanostructures, hierarchical architecture materials with large surface area can facilitate lithium ions transport. And the large cavities among the nano-sized particles of the hierarchical framework can alleviate volume strain and stabilize the structure during the intercalation-deintercalation processes.^[24–26] Efficient and effective transportation of lithium ions and electrons is considered as the key factor for improving the rate capacity and enhancing long-term cycle life. The addition of inactive and insulating binders makes sure that active material can adhere to the current collectors, however, it blocks the pathway of the lithium ions diffusion and causes inferior conductivity. Therefore, it is reasonable to directly fabricate hierarchical Co₃O₄ materials on current collectors to form binder-free electrodes. Wu *et al.* prepared Co₃O₄ nanowire arrays on Ti foil and the diameter of the nanowire was about 500 nm. The as-prepared Co₃O₄ nanowires exhibited a stable capacity of 700 mAh·g⁻¹ after 20 cycles at 111 mA·g⁻¹.^[27] Therefore, *in-situ* growth can make better connection between active materials and current collectors than traditional electrode fabrication.

In this paper, we fabricated one-dimensional hierarchical Co₃O₄ nanowires on nickel foam *via* a simple hydrothermal method. Subsequently, after thermal annealing in air, they were directly applied as anode for LIBs. The nanowires are composed of ultra-small nano-particles (about 10 nm) and self-assembled into a hierarchical architecture. The diameter is ~160 nm. For comparison, we also systematically investigated the growth mechanism of hierarchical Co₃O₄ nanowires by controlling hydrothermal reaction time and the effects of reaction conditions on material morphologies. These structures exhibit different electrochemical performances when they are used as anodes in LIBs. As we expected, hierarchical nanowires electrode exhibits high capacity owing to the unique hierarchical architecture that enhances contact area between electrode and electrolyte. This indicates the potential application of hierarchical Co₃O₄ nanowires as anode materials for LIBs.

Experimental

Materials synthesis

The hierarchical Co₃O₄ nanowires were fabricated by a thermal annealing-induced phase transformation from a morphology-similar precursor synthesized by hydrothermal method. All the reagents used were of AR grade and were not purified further. Deionization (DI) water was used throughout the experiment. Firstly, cobalt nitrate hexahydrate (Co(NO₃)₂•6H₂O), sodium chloride and urea (CO(NH₂)₂) were dissolved in 37 mL water, and then ammonium fluoride (NH₄F) was added in the above mixed solution under stirring for 5 min. Afterwards, a piece of nickel foam (1 cm×1 cm) was immersed into the mixed solution. The autoclave was

kept at 160 °C for different time after sealed. Then it was cooled to room temperature. The substrate was then taken out of the solution and rinsed with distilled water and cleaned in alcohol by ultrasonic for several times. Then it was annealed at 350 °C (with a ramping rate of 2 °C·min⁻¹) for 2 h in the air.

Materials characterizations

The crystal structure and phase composition of the as-prepared products were characterized with X-ray diffraction (XRD; BRUKER-AXS, D8 ADVANCE, under Cu K α radiation $\lambda=0.1542$ nm, at 40 kV and 100 mA). The morphologies and microstructures of the products were examined by a field-emission scanning electron microscope (FESEM; FEI, Quanta FEG 250, operated at 10 kV) and transmission electron microscopy (TEM; JEOL, JEM-2100, 200 kV, with electron diffraction).

Electrochemical measurements

The battery performance of hierarchical Co₃O₄ nanowires was evaluated using a battery testing system LAND CT2001 (Wuhan LAND Electronics, China) with a cutoff voltage range (0.01 to 3.0 V, vs. Li⁺/Li). The electrochemical tests were investigated using a coin-type half cell (CR2025). Metallic lithium was used as the counter/reference electrode and a polypropylene microporous membrane (Celgard 2400) was used as the separator. The electrolyte was composed of 1 mol·L⁻¹ LiPF₆-ethylene carbonate (EC)-dimethyl carbonate (DMC)-ethylmethyl carbonate (EMC) (1 : 1 : 1 by volume). Coin cells were assembled using a compact hydraulic crimping machine (MSK-110, MTI Corporation) in an argon-filled glove-box (Universal 2400/750/900, MIKROUNA) with oxygen and water lower than 0.1 mg·L⁻¹. Cyclic voltammetry (CV) was performed on a Zahner/Zennium electrochemical workstation in the potential range 0.01–3.0 V (vs. Li⁺/Li) at a scanning rate of 0.1 mV·s⁻¹ at room temperature. For the electrochemical impedance spectroscopy (EIS) measurements, the excitation voltage applied to the cell was 5 mV and the frequency range was from 100 kHz to 0.01 Hz.

Results and Discussion

The morphology and dimension of the Co₃O₄ nanowires are characterized with FE-SEM. Both the hydrothermal reaction time and dosage of Co(NO₃)₂•6H₂O affect the formation of the final Co₃O₄ structures. A tunable morphology can be controlled grown by changing hydrothermal time. Through optimizing the hydrothermal reaction time, different Co₃O₄ nanowire morphologies have been synthesized. Figures 1a—1d depict the SEM images of the products after different reaction times, and the dosage of Co(NO₃)₂•6H₂O is 1.6 mmol. Herein, the morphologies under different reaction times indicate the regulation of formation processes. A dense

layer formed in a shorter time (0.5 h) can be observed (Figure 1a). With the growth from the feedstock, nanowires emerge from the bonding sites of the dense layer. As the reaction time is prolonged, nanowires with length of several micrometers that grow on the nickel foam become denser with a random orientation. Each wire has a sharp tip and the diameter is in the range 85–100 nm with the length more than 10 μm (Figure S1).

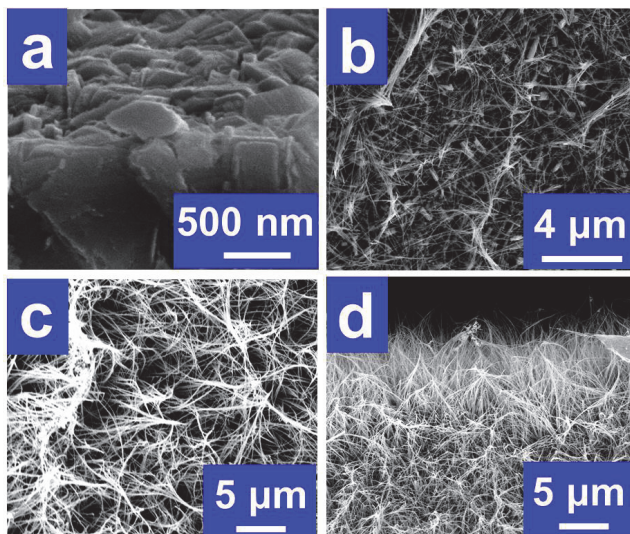


Figure 1 SEM images of Co_3O_4 with different morphology on nickel foam synthesized at 160 $^{\circ}\text{C}$ for different hydrothermal reaction times (dosage of $\text{Co}(\text{NO}_3)_2 \cdot 6\text{H}_2\text{O}$: 1.6 mmol): (a) 0.5 h; (b) 3 h; (c) 6 h; (d) 12 h.

Figure 2 shows the XRD patterns of the sample for different hydrothermal reaction times, and the dosage of $\text{Co}(\text{NO}_3)_2 \cdot 6\text{H}_2\text{O}$ is 1.6 mmol. All the diffraction peaks could be well indexed to the standard XRD data for Co_3O_4 (JCPDS No. 42—1647), except for the three peaks (marked by ◆) ascribed to the nickel foam substrate. The XRD pattern demonstrates that the as-synthesized sample on nickel foam is pure cobalt oxide.^[8] It indicates that crystalline Co_3O_4 phase has been formed without any impurities after calcination. The obtained samples can be directly employed as the working electrode by preparing coin-type half cells and Li foil as the counter/reference electrode.

The three samples with nanowires are evaluated using a standard coin cell. The electrochemical performances of them cycled at 500 $\text{mA} \cdot \text{g}^{-1}$ are depicted in Figure 3. From the galvanostatic charge-discharge curves of the cells, it is observed that all cells exhibit a high initial discharge capacity, which is significantly higher than the theoretical value ($890 \text{ mAh} \cdot \text{g}^{-1}$). The initial discharge capacity of 6 h sample is about $1550 \text{ mAh} \cdot \text{g}^{-1}$ that is the lower than that of the others. However, the 6 h sample exhibits a stable capacity $780 \text{ mAh} \cdot \text{g}^{-1}$ after 100 cycles at 500 $\text{mA} \cdot \text{g}^{-1}$. All the performances are not ideal. That may be due to the large axial diameter ratio caused by low concentration of the feedstock. The capacity fading after about 30 cycles

could be due to the fact that the high discharge/charge current density might induce drastic structure reorganization accompanied by decomposition and reformation of the electrolyte.^[28,29] The expansion during the charge-discharge processes leads to the fracture of the nanowire and it is falling off from the dense layer.

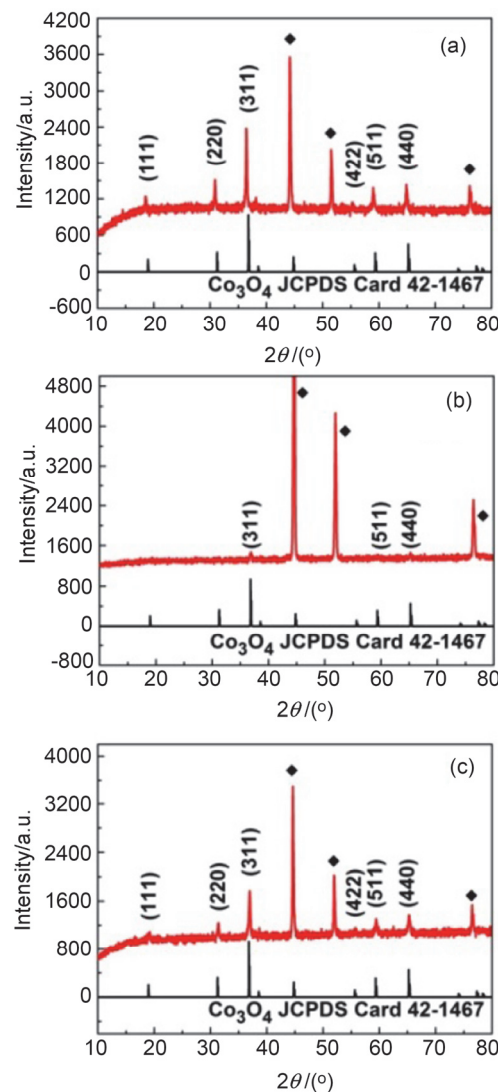


Figure 2 XRD patterns of Co_3O_4 for different hydrothermal reaction times (dosage of $\text{Co}(\text{NO}_3)_2 \cdot 6\text{H}_2\text{O}$: 1.6 mmol): (a) 3 h; (b) 6 h; (c) 12 h.

In order to enhance the crystallinity and reduce the axial diameter ratio of the nanowires, the dosage of $\text{Co}(\text{NO}_3)_2 \cdot 6\text{H}_2\text{O}$ is changed to 2.4 mmol. As shown in Figures 4a–4c, the SEM images at different magnification of the samples are obtained. Figure 4a implies that the surface of nickel foam is uniformly covered with Co_3O_4 nanowires with a length of 5–7 μm . According to Figure 4b, the diameter of the nanowires is not homogeneous. Figure 4c shows a magnified SEM image of several nanowires with a diameter 90–150 nm. The axis-to-diameter ratio is smaller than that of previous samples. TEM image (Figure 4d) shows that the nano-

wire is composed of ultra-small nanoparticles of ~ 10 nm, demonstrating a hierarchical structure. Mesopores among the nanoparticles can be clearly identified. The high-resolution TEM (HR-TEM) image shown in Figure 4e reveals that numerous nanoparticles in the Co_3O_4 nanowire are interconnected with each other. Besides, size of the irregular mesopores among the nanoparticles is about 5 nm. The interplanar spacing in the HR-TEM is 0.202 nm, corresponding to the (400) plane of Co_3O_4 crystals. The distinct diffraction spots in the selected area electron diffraction (SAED) pattern (Figure 4f) indicate that the Co_3O_4 nanowire is polycrystalline.

Figure 5 shows the XRD patterns of the sample with hydrothermal treatment for 6 h, and the dosage of $\text{Co}(\text{NO}_3)_2 \cdot 6\text{H}_2\text{O}$ is 2.4 mmol. The diffraction peaks at 31.3° , 36.8° , 55.65° , 59.4° and 65.2° can be perfectly indexed to (220), (311), (422), (511) and (440) planes of cubic Co_3O_4 (JCPDS No. 42 – 1647), respectively. Nickel foam is coated by the dense layer composed of the precursors, which prevent Ni from being oxidized. The XRD pattern demonstrates that the as-synthesized sample on nickel foam is pure cobalt oxide.^[8] It indicates that crystalline Co_3O_4 phase has been formed without any impurities after calcination.

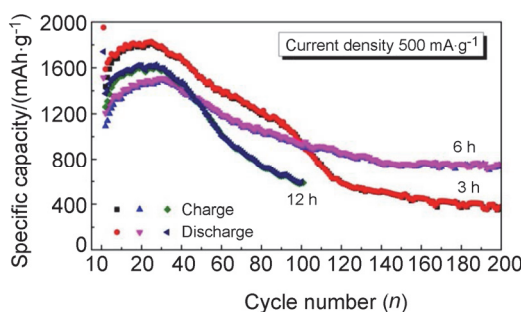


Figure 3 Cycling performance of Co_3O_4 nanowires synthesized at different times and the corresponding electrodes cycled at $500 \text{ mA}\cdot\text{g}^{-1}$.

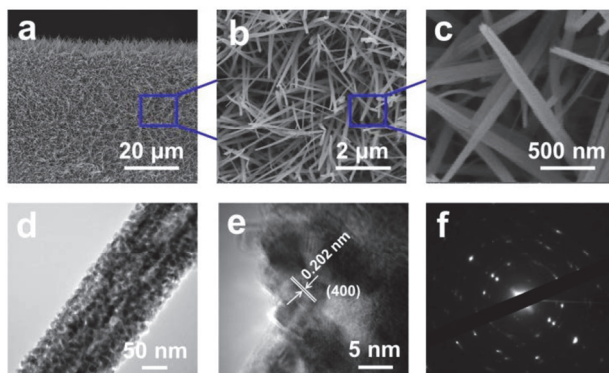


Figure 4 (a, b, c) SEM images of the Co_3O_4 nanowires at different resolutions (dosage of $\text{Co}(\text{NO}_3)_2 \cdot 6\text{H}_2\text{O}$: 2.4 mmol); (d) TEM image, (e) HR-TEM image and (f) SAED patterns of the nanowire.

Figure 6 shows the galvanostatic charge-discharge curve of Co_3O_4 nanowires with hydrothermal treatment

for 6 h tested at $500 \text{ mA}\cdot\text{g}^{-1}$ (a voltage window of 0.01 – 3.0 V). The tendency of the initial cycles is inconsistent with the previous samples. The discharge capacity experiences a gradual increase in the initial 20 cycles, followed by a fading tendency for 10 cycles. Then it stabilizes at $957 \text{ mAh}\cdot\text{g}^{-1}$ after 100 cycles.^[13,30] The increasing capacity of the electrode in the first 20 cycles may be due to an activation process caused by the enlarged surface area after a nanosize effect.^[28,31,32] The stable discharge capacity may owe to the hierarchical Co_3O_4 nanowire structure. The capacity lost in the following 10 cycles may result from the deterioration of the hierarchical structure, which is an inherent characteristic for the transition metal oxide electrodes. The rate performance of LIBs anodes is a decisive factor, especially for high-power applications in power grids. The SEM and TEM images of the Co_3O_4 nanowire arrays electrode after discharging/charging up to 100 cycles at a current density of $500 \text{ mA}\cdot\text{g}^{-1}$ are also characterized as shown in Figure S2. We can find the increased roughness on the electrode surface and some expansion and merging of branches caused by the redox reaction during the repeated charge/discharge processes.

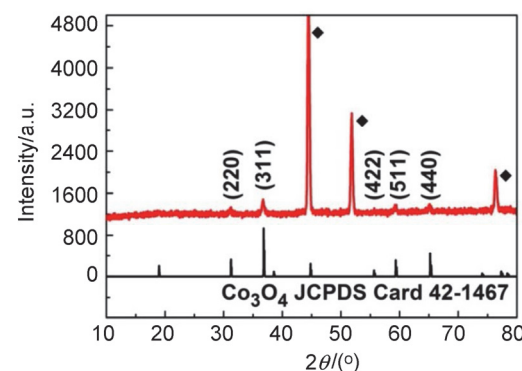


Figure 5 XRD pattern of the as-prepared nanowires on the nickel foam (dosage of $\text{Co}(\text{NO}_3)_2 \cdot 6\text{H}_2\text{O}$: 2.4 mmol, reaction time: 6 h).

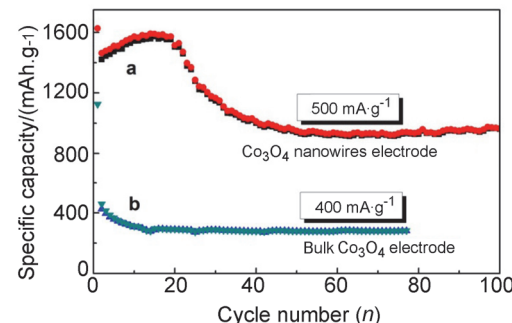


Figure 6 (a) Cycling performance of Co_3O_4 nanowires electrode at $500 \text{ mA}\cdot\text{g}^{-1}$ (dosage of $\text{Co}(\text{NO}_3)_2 \cdot 6\text{H}_2\text{O}$: 2.4 mmol, reaction time: 6 h); (b) cycling performance of bulk Co_3O_4 at $400 \text{ mA}\cdot\text{g}^{-1}$.

To further characterize the cycling stability of the hierarchical Co_3O_4 nanowires electrode, cycling tests

were performed at a current rate of $1000 \text{ mA}\cdot\text{g}^{-1}$ under ambient conditions. Figure 7 shows the galvanostatic charge-discharge curves of the cell up to 90 cycles. The tendency is inconsistent with that observed in the cycling at $500 \text{ mA}\cdot\text{g}^{-1}$. The reversible discharge capacity can remain at about $612 \text{ mAh}\cdot\text{g}^{-1}$ after 90 cycles. Then the current density was changed to $500 \text{ mA}\cdot\text{g}^{-1}$. The tendency of the curve means the increase of reversible capacity. The capacity stabilizes at about $900 \text{ mAh}\cdot\text{g}^{-1}$ after 170 cycles, with a coulombic efficiency of almost 100%.

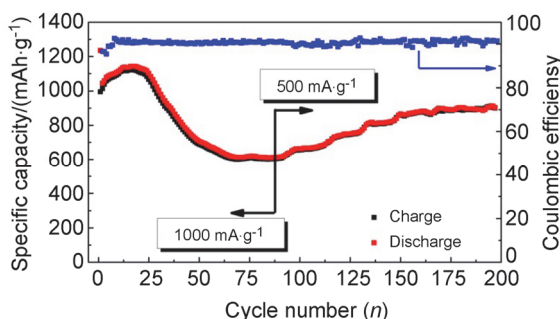


Figure 7 Cycling performance of Co_3O_4 nanowires electrode cycled at $1000 \text{ mA}\cdot\text{g}^{-1}$ for 90 cycles and at $500 \text{ mA}\cdot\text{g}^{-1}$ for 110 cycles (dosage of $\text{Co}(\text{NO}_3)_2\cdot 6\text{H}_2\text{O}$: 2.4 mmol, reaction time: 6 h).

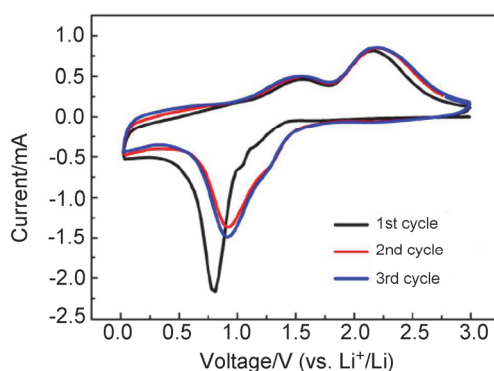


Figure 8 CV curves of Co_3O_4 nanowires electrode at a scan rate of $0.1 \text{ mV}\cdot\text{s}^{-1}$ for the first three cycles.

The electrochemical performance of LIBs anode made from the binder-free Co_3O_4 nanowires was evaluated by cyclic voltammetry (CV). A cyclic voltammogram collected at a scan rate of $0.1 \text{ mV}\cdot\text{s}^{-1}$ between 0.01 and 3.0 V is shown in Figure 8. In the first cycle, the small irreversible peak at about 1.0 V should be ascribed to lithium insertion into the crystal structure of the Co_3O_4 without structural change ($\text{Co}_3\text{O}_4 + x\text{Li}^+ + x\text{e}^- \rightarrow \text{Li}_x\text{Co}_3\text{O}_4$), and the latter sharp reduction peak located at 0.8 V is owing to the complete reduction from Co^{3+} to $\text{Co}(0)$ and the formation of a solid-electrolyte-interphase (SEI) layer. This reduction reaction has a significant effect on the reversible capacity of Co_3O_4 .^[29] The full lithiation voltage in the following cycles (about 0.93 V) is higher than that in the first cycle (about 0.8 V), probably due to the improved kinetics of the hierarchical Co_3O_4 nanowires electrode resulting from a mi-

crostructural alteration after the first lithiation. During the anodic polarization process, the curves present a pair of broad redox peaks at around 1.5/2.1 V. The potential interval (ΔE) is representative of the kinetic process, especially considering that the electrochemical process involves lithium diffusion in the solid phase and electron jumping across the electrodes.^[33] It is associated with the oxidation reactions and conversion of metallic cobalt into cobalt oxide. The overlapping of the CV curves in the subsequent cycles indicates good reversibility of the electrochemical reactions, and this is further confirmed by the following cycling performance test.

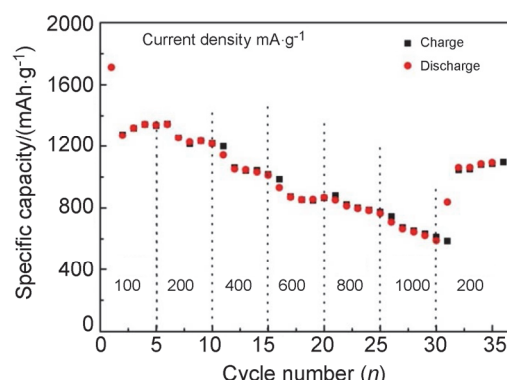


Figure 9 Rate performance of Co_3O_4 nanowires electrode (dosage of $\text{Co}(\text{NO}_3)_2\cdot 6\text{H}_2\text{O}$: 2.4 mmol, reaction time: 6 h).

Figure 9 shows the durable and stable rate capacity of the Co_3O_4 nanowires with hydrothermal treatment for 6 h at different current densities. When cycled at the current densities of 100, 200, 400, 600, 800, 1000 and 200 $\text{mA}\cdot\text{g}^{-1}$, the electrode delivers discharge capacities of 1276.2, 1233.4, 1051.5, 855.9, 796.4, 666 and 1060.1 $\text{mAh}\cdot\text{g}^{-1}$, respectively. Importantly, a high capacity of 1060.1 $\text{mAh}\cdot\text{g}^{-1}$ can be recovered rapidly when the current rate is reduced again from $1000 \text{ mA}\cdot\text{g}^{-1}$ to $200 \text{ mA}\cdot\text{g}^{-1}$. The good rate capability implies that the direct attachment and the dense layer on the nickel foam can enhance the fast charge transfer pathways. The existences of the void space between Co_3O_4 nanowires can expand the electrochemically active area, facilitating the diffusion of lithium ions.

Electrochemical impedance spectroscopy (EIS) is carried out to investigate the changing of the charge transfer resistance during cycling. The impedance spectra of the battery cycles after different times were performed, as shown in Figure 10. Given transition metal oxide materials, the semicircular pattern in the high frequency region may be related to the solid electrolyte interphase film resistance and charge-transfer resistance.^[34–36] The diameter of the semicircle part is decreased with the prolonged cycles, which also demonstrates the good contact between nanowires and substrate during cycles. It indicates that the hierarchical Co_3O_4 nanowires provide efficient lithium diffusion tunnels and improve charge-transfer kinetics.

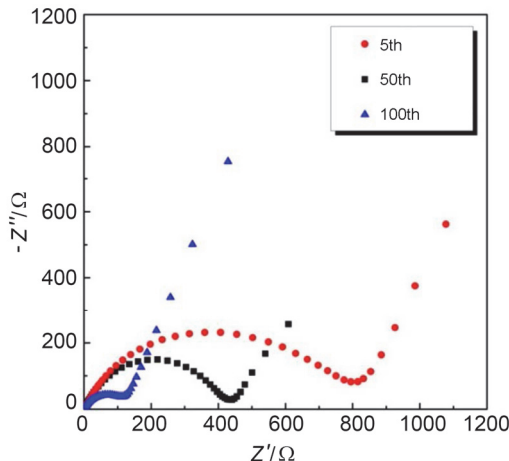


Figure 10 Nyquist plots of Co_3O_4 nanowires electrode after different cycles in the frequency range between 100 Hz and 100 mHz.

Conclusions

In summary, hierarchical Co_3O_4 nanowires directly on nickel foam have been successfully fabricated and good cycle performance was obtained when investigated as LIBs anode. The nanowires on the nickel foam with a length of 5–7 μm are composed of numerous ultra-small nanoparticles of about ~10 nm. A stable reversible capacity 957 $\text{mAh}\cdot\text{g}^{-1}$ is obtained when cycled at 500 $\text{mA}\cdot\text{g}^{-1}$ after 100 cycles without fading. That may owe to good contact of nanowires with nickel foam and fast electron transfer from nanowires to substrate. The hierarchical structure facilitates lithium ion diffusion, prevents the collapse of the structure and improves charge-transfer kinetics during the cycles. The good electrochemical performance of Co_3O_4 makes it a promising anode for rechargeable LIBs.

Acknowledgement

This work is supported by the National Natural Science Foundation of China (Nos. 51501072, 51472110, 11174112), the Fund for the Excellent Young and Middle-aged Scientists of Shandong Province (No. BS2014CL026), the Doctoral Foundation from University of Jinan (No. XBS1448) and the Shandong Provincial Natural Science Foundation (No. JQ201214). The research programs from the Ministry of Education, China, are also acknowledged (Nos. NCET-11-1027, 213021A).

References

- [1] Tang, W.; Zhu, Y. S.; Hou, Y. Y.; Liu, L. L.; Wu, Y. P.; Loh, K. P.; Zhang, H. P.; Zhu, K. *Energy Environ. Sci.* **2013**, *6*, 2093.
- [2] Zaghib, K.; Mauger, A.; Groult, H.; Goodenough, J. B.; Julien, C. M. *Materials* **2013**, *6*, 1028.
- [3] Ou, J. K.; Yang, L.; Zhang, Y. Z.; Chen, L.; Guo, Y.; Xiao, D. *Chin. J. Chem.* **2015**, *33*, 1293.
- [4] Chen, H. X.; Zhang, Q. B.; Wang, J. X.; Xu, D. G.; Li, X. H.; Yang, Y.; Zhang, K. L. *J. Mater. Chem. A* **2014**, *2*, 8483.
- [5] Hua, W. B.; Wang, Y. J.; Zhong, Y. J.; Wang, G. P.; Zhong, B. H.; Fang, B. Z.; Guo, X. D.; Liao, S. X.; Wang, H. J. *Chin. J. Chem.* **2015**, *33*, 261.
- [6] Zhang, Q. B.; Wang, J. X.; Dong, J. C.; Ding, F.; Li, X. H.; Zhang, B.; Yang, S. H.; Zhang, K. L. *Nano Energy* **2015**, *13*, 77.
- [7] Ellis, B. L.; Knauth, P.; Djennizian, T. *Adv. Mater.* **2014**, *26*, 3368.
- [8] Huang, F.; Zhan, H.; Zhou, Y. H. *Chin. J. Chem.* **2003**, *21*, 1275.
- [9] Mitsch, T.; Krämer, Y.; Feinauer, J. L.; Gaiselmann, G.; Markötter, H. N.; Manke, I.; Hintennach, A.; Schmidt, V. *Materials* **2014**, *7*, 4455.
- [10] Liu, D. H.; Zhang, C.; Lv, X. H.; Zheng, X. Y.; Zhang, L.; Zhi, L. J.; Yang, Q. H. *Chin. J. Chem.* **2015**, DOI: 10.1002/cjoc.201500321.
- [11] Pei, Y.; Wang, S.; Zhou, Q.; Xie, S. H.; Qiao, M. H.; Jiang, Z. Y.; Fan, K. N. *Chin. J. Chem.* **2007**, *25*, 1385.
- [12] Liu, J. H.; Chen, J. S.; Wei, X. F.; Lou, X. W.; Liu, X. W. *Adv. Mater.* **2011**, *23*, 998.
- [13] Zhang, Q. B.; Chen, H. X.; Wang, J. X.; Xu, D. G.; Li, X. H.; Yang, Y.; Zhang, K. L. *ChemSusChem* **2014**, *7*, 2325.
- [14] Yuan, C. Z.; Wu, H. B.; Xie, Y.; Lou, X. W. *Angew. Chem., Int. Ed.* **2014**, *53*, 1488.
- [15] Sun, Y. M.; Hu, X. L.; Luo, W.; Huang, Y. H. *J. Mater. Chem.* **2012**, *2*, 13826.
- [16] Guan, H.; Wang, X.; Li, H. Q.; Zhi, C. Y.; Zhai, T. Y.; Bando, Y.; Golberg, D. *Chem. Commun.* **2012**, *48*, 4878.
- [17] Li, D. H.; Yang, D. J.; Zhu, X. Y.; Jing, D. W.; Xia, Y. Z.; Ji, Q.; Cai, R. S.; Lia, H. L.; Che, Y. K. *J. Mater. Chem. A* **2014**, *2*, 18761.
- [18] Luo, J. S.; Xia, X. H.; Luo, Y. S.; Guan, C.; Liu, J. L.; Qi, X. Y.; Ng, C. F.; Yu, T.; Zhang, H.; Fan, H. J. *Adv. Energy Mater.* **2013**, *3*, 737.
- [19] Cao, K. Z.; Jiao, L. F.; Liu, H. Q.; Liu, Y. C.; Wang, Y. J.; Guo, Z. P.; Yuan, H. T. *Adv. Energy Mater.* **2015**, *5*, 1401421.
- [20] Zhang, Q. B.; Chen, H. X.; Han, X.; Cai, J. J.; Yang, Y.; Liu, M. L.; Zhang, K. L. *ChemSusChem* **2015**, DOI: 10.1002/cssc.201501151.
- [21] Liu, J.; Wan, Y. L.; Liu, C. P.; Liu, W.; Ji, S. M.; Zhou, Y. C.; Wang, J. B. *Eur. J. Inorg. Chem.* **2012**, *1*, 3825.
- [22] Sun, H. Y.; Liu, Y. G.; Yu, Y. L.; Ahmad, M. K.; Nan, D.; Zhu, J. *Electrochim. Acta* **2014**, *118*, 1.
- [23] Peng, L.; Feng, Y. Y.; Bai, Y. J.; Qiu, H. J.; Wang, Y. J. *Mater. Chem. A* **2015**, *3*, 8825.
- [24] Li, X. Y.; Huang, X. L.; Liu, D. P.; Wang, X.; Song, S. Y.; Zhou, L.; Zhang, H. J. *J. Phys. Chem. C* **2011**, *115*, 21567.
- [25] Xiao, Y. H.; Liu, S. J.; Li, F.; Zhang, A. Q.; Zhao, J. H.; Fang, S. M.; Jia, D. Z. *Adv. Funct. Mater.* **2012**, *22*, 4052.
- [26] Zhang, Z. C.; Li, L.; Xu, Q.; Cao, B. Q. *RSC Adv.* **2015**, *5*, 61631.
- [27] Li, Y.; Tan, B.; Wu, Y. *Nano Lett.* **2008**, *8*, 265.
- [28] Xiong, S.; Chen, J.; Lou, X. W.; Zeng, H. *Adv. Funct. Mater.* **2012**, *22*, 861.
- [29] Mei, W. M.; Huang, J.; Zhu, L. P.; Ye, Z. Z.; Mai, Y. J.; Tu, J. P. *J. Mater. Chem.* **2012**, *22*, 9315.
- [30] Li, J. F.; Xiong, S. L.; Liu, Y. R.; Ju, Z. C.; Qian, Y. T. *ACS Appl. Mater. Interfaces* **2013**, *5*, 981.
- [31] Lee, K. J.; Kim, T. H.; Kim, T. K.; Lee, J. H.; Song, H. K.; Moon, H. R. *J. Mater. Chem. A* **2014**, *2*, 14393.
- [32] Zheng, F. C.; Zhu, D. Q.; Chen, Q. W. *ACS Appl. Mater. Interfaces* **2014**, *6*, 9256.
- [33] Croce, F.; Epifanio, A. D.; Hassoun, J.; Deptula, A.; Olczac, T.; Serosati, B. *Electrochem. Solid-State Lett.* **2002**, *5*, A47.
- [34] Kang, Y. M.; Song, M. S.; Kim, J. H.; Kim, H. S.; Park, M. S.; Lee, J. Y.; Liu, H. K.; Dou, S. X. *Electrochim. Acta* **2005**, *50*, 3667.
- [35] Kim, G. P.; Park, S.; Nam, I.; Park, J.; Yi, J. J. *Mater. Chem. A* **2013**, *1*, 3872.
- [36] Huang, X. B.; Li, X.; Wang, H. Y.; Pan, Z. L.; Qu, M. Z.; Yu, Z. L. *Electrochim. Acta* **2010**, *55*, 7362.

(Lu, Y.)